A Multiloop Concentric Hyperthermia Applicator with Enhanced Penetration Depth

P. G. COTTIS, NIKOLAOS K. UZUNOGLU, MEMBER, IEEE, AND G. E. CHATZARAKIS

Abstract —**The electromagnetic field deposition into a three-layer cylindrical human body model by a multiloop concentric hyperthermia applicator is investigated analytically. The multiloop radiator axis is taken to be coincident with the cylinder axis. A technique based on the method of separation of variables is employed to determine the axisymmetric field in every point. In order to compute the imposed specific absorption rate in the tissues, a numerical integration technique is utilized. Numerical results are presented for several loop geometries at a 13 MHz operation frequency. The possibility of obtaining improved in-depth heating in comparison with conventional single magnetic loop applicators is investigated. It is shown that significant enhancement of the penetration depth can be obtained by using a simple phased magnetic loop system.**

I. Introduction

HEATING OF MALIGNANT human tissues, a therapeutic technique known as hyperthermia, is being increasingly used by many researchers [1]. One of the more common regional hyperthermia systems being evaluated in practice is the magnetrode [2], [3], which is basically a circumferential magnetic loop radiator centered on the long axis of the patient. The azimuthal symmetry of the excitation leads to a zero electric field on the axis of the loop. The magnetic mode character of the electromagnetic field permits a relatively deep half-power penetration depth of approximately 5 cm at 13 MHz for common torso size. Another reported advantage of the loop radiator in comparison with capacitive type electrodes is the mild heating of superficial fat layers because of the absence of normal electric field components on the body surface. However, considering the requirement for heating deep-seated tumors it is desirable to improve the penetration depth of this type of antenna.

The development of a family of radio-frequency helical coil applicators which produce transversely uniform axially distributed heating in cylindrical fat-muscle phantoms has been investigated experimentally by Ruggera and Kantor [4].

The field distribution of a magnetrode radiator of finite length encircling the human body has been analyzed by Elliott *et al.* [2] by applying an approximate theory. It is shown that the field distribution in the plane of a finite height magnetic cylinder is intermediate between what would be expected for an infinitely long solenoid and a single turn of wire. A two-dimensional nonhomogeneous model has been used by Hill *et al.* [5] to calculate the electric field for a magnetic loop antenna.

In this paper a three-layer cylindrical human body model is proposed for the computation of the electromagnetic field distribution inside the human body excited by a multiloop axisymmetric magnetic mode radiator. The three layers of the cylinder correspond to muscle, fat, and skin. The common loop antenna axis is taken to be coincident with the cylindrical model axis. The axial symmetry of the excitation leads to an axisymmetric field distribution and simplifies the analysis considerably. A separation-of-variables technique is employed to obtain the electromagnetic field expressions in each region and then the boundary conditions on the layer interfaces are satisfied. The derived field expressions are complex Sommerfeld-type integrals [6]. In order to compute these integrals, numerical techniques are employed. Emphasis is given to the enhancement of power penetration within the cylindrical body by using phased-array principles. In this context several loop current phase and amplitude distributions are investigated. This approach bears similarities to other phased-array regional hyperthermia techniques already discussed in the literature [1].

In the following analysis an $\exp(-j\omega t)$ time dependence is assumed for the field quantities and it is suppressed throughout the analysis. Furthermore the whole space is assumed to be magnetically homogeneous, with a magnetic permeability equal to the free-space value $\mu = \mu_0 = 4\pi \times 10^{-7}$ H/m.

II. Mathematical Formulation of the Problem

In Fig. 1 the geometry of the three-layer cylinder encircled with several loop radiators is illustrated. The core medium corresponds to muscle tissues while the outer layers represent the fat and skin tissues. The relative complex permitivities of the layers are shown with ϵ_i, $i = 1,2,3$ ($\epsilon_i = \epsilon_{r_i} + j\sigma_i/(\omega\epsilon_0)$). The layer boundaries are on the $\rho = a$ and $\rho = b$ cylinder surfaces. The outer body surface is at $\rho = c$. The electromagnetic properties of the space exterior to the cylinder are taken to be those of free space; i.e., $\epsilon_0 = 10^{-9}/(36\pi)$ (F/m) and $\mu_0 = 4\pi \times 10^{-7}$

Manuscript received July 10, 1987; revised October 27, 1987.

The authors are with the Department of Electrical Engineering, National Technical University of Athens, Athens 10682, Greece.

IEEE Log Number 8719206.

0018-9480/88/0400-0676$01.00 ©1988 IEEE

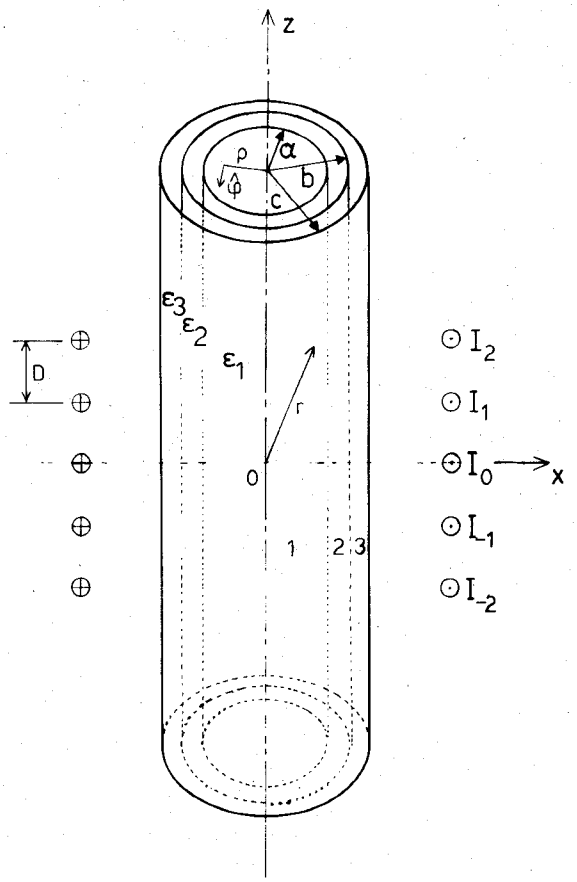

Fig. 1. Three-layer cylindrical human body model irradiated by a multiloop magnetic type antenna.

(H/m). Each radiating loop element is assumed to be on the cylindrical surface at $\rho = \rho_n$. Then the position of each antenna is defined by the distance from the $z = 0$ plane; that is, the nth loop coordinates are $\rho = \rho_n$, $z = z_n$. The electric currents flowing in the loops are taken to be $I_n = |I_n| \angle \phi_n$. Therefore the spatial current density distribution (A/m^2) is expressed in the following form:

$$\boldsymbol{J}(\rho, z) = \hat{\varphi} \sum_{n=-N}^{N} I_n \delta(\rho - \rho_n)\delta(z - z_n) \tag{1}$$

where $2N+1$ is the number of loops, $\hat{\varphi}$ is the unit vector as shown in Fig. 1, and $\delta(x)$ is the delta function. Because of the azimuthal symmetry of the current density it is readily deduced that the corresponding electric field should have a single component along the $\hat{\varphi}$ vector, that is,

$$\boldsymbol{E}(\rho, z) = \hat{\varphi}\psi(\rho, z). \tag{2}$$

The electric field should also satisfy the wave equation

$$\nabla \times \nabla \times \boldsymbol{E}(\rho, z) - k_0^2 \epsilon_i \boldsymbol{E}(\rho, z) = j\omega\mu_0 \boldsymbol{J}(\rho, z) \tag{3}$$

where $k_0 = \omega\sqrt{\epsilon_0\mu_0}$, $i = 1,2,3,4$, depending on the position of the observation point $\boldsymbol{r}$ (see Fig. 1) and $\epsilon_4 = 1$. Substituting (2) into (3) and performing some trivial operations, a scalar wave equation is obtained as follows:

$$\nabla^2\psi_i(\rho, z) - \frac{1}{\rho^2}\psi_i(\rho, z) + k_0^2\epsilon_i\psi_i(\rho, z) = -j\omega\mu_0\hat{\varphi}\cdot\boldsymbol{J}(\rho, z) \tag{4}$$

where again $i = 1$, 2, 3, and 4. The subscript in $\psi_i(\rho, z)$ denotes the layer in which the field is computed.

In (4) the right-hand side consists of the superposition of $M = 2N+1$ independent loop currents. Therefore the linear nature of the problem permits us to solve the problem by considering only a single loop and then superimposing the M independent solutions to obtain the overall response.

Assuming a $\boldsymbol{J}\cdot\hat{\varphi} = \delta(\rho - \rho_n)\delta(z - z_n)$ excitation in the right-hand side of (4), the electric field for the inner layers can be easily written in terms of cylindrical wave functions as follows:

$$\psi_1(\rho, z) = \frac{1}{2\pi}\int_{-\infty}^{+\infty} dk e^{jk(z-z_n)} A_1(k) J_1(\lambda_1\rho) \qquad \text{for } 0 < \rho < a \tag{5}$$

$$\psi_2(\rho, z) = \frac{1}{2\pi}\int_{\infty}^{\infty} dk e^{jk(z-z_n)} \big(A_2(k)J_1(\lambda_2\rho) + B_2(k)Y_1(\lambda_2\rho)\big) \qquad \text{for } a < \rho < b \tag{6}$$

$$\psi_3(\rho, z) = \frac{1}{2\pi}\int_{-\infty}^{+\infty} dk e^{jk(z-z_n)} \big(A_3(k)J_1(\lambda_3\rho) + B_3(k)Y_1(\lambda_2\rho)\big) \qquad \text{for } b < \rho < c \tag{7}$$

where $\lambda_i = (k_0^2\epsilon_i - k^2)$, $i = 1,2,3$, and $A_i(k)$ and $B_i(k)$ are unknown coefficients to be determined. Notice that in the core region only the Bessel function $J_1(x)$ is included, since the Neumann function $|Y_1(x)| \to \infty$ as $x \to 0$.

The solution of (4) in the region outside the cylinder is more complicated than the previous solutions because of the presence of the nonhomogeneous term, $-j\omega\mu_0\delta(\rho - \rho_n)\delta(z - z_n)$, in the right-hand side of (4). Therefore the solution can be decomposed into two terms, corresponding to the primary field in the absence of the cylinder and to the secondary field due to the reflection from the cylindrical object. The corresponding solutions are denoted by ψ_0 and ψ_s, respectively. The former field should satisfy the nonhomogeneous wave equation

$$\nabla^2\psi_0(\rho, z) - \left(\frac{1}{\rho^2} - k_0^2\right)\psi_0(\rho, z) = -j\omega\mu_0\delta(\rho - \rho_n)\delta(z - z_n) \tag{8}$$

and therefore $\psi_0(\boldsymbol{r})$ is equal to the free-space Green's function for a loop antenna excitation. Then, following a standard procedure for computing the Green's functions of differential operators [7], the primary field is found to be

$$\psi_0(\rho, z) = -\frac{j\omega\mu_0\rho_n}{2\pi}\int_{-\infty}^{+\infty} dk e^{jk(z-z_n)} \begin{cases} I_1(\mu\rho)K_1(\mu\rho_n) & \text{for } \rho < \rho_n \\ I_1(\mu\rho_n)K_1(\mu\rho) & \text{for } \rho > \rho_n \end{cases} \tag{9}$$

where

$$\mu = \left(k_0^2 - k^2\right)^{1/2} \tag{10}$$

and $I_1(x)$ and $K_1(x)$ are the modified Bessel and Hankel functions, respectively. Observe that as $\rho \to \infty$, $\psi_0(\rho, z)$

should satisfy the Sommerfeld–Müller radiation conditions. Therefore the double-valued function μ is defined so that $\mathrm{Re}(\mu) > 0$ and $\mathrm{Im}(\mu) > 0$.

The same arguments hold for the secondary field. Therefore

$$\psi_s(\rho, z) = \frac{1}{2\pi}\int_{-\infty}^{+\infty} dk\, e^{jk(z-z_n)} A_4(k) K_1(\mu\rho) \quad (11)$$

where again $A_4(k)$ is an unknown coefficient to be determined.

The solutions given above in (5)–(7), (9), and (11) should satisfy the boundary conditions for the continuity of the tangential electric and magnetic fields at the layer interfaces $\rho = a$, $\rho = b$, and $\rho = c$.

The following boundary conditions should be satisfied:

$$\psi_1 = \psi_2; \qquad \frac{\partial\psi_1}{\partial\rho} = \frac{\partial\psi_2}{\partial\rho} \qquad \text{at } \rho = a \quad (12)$$

$$\psi_2 = \psi_3; \qquad \frac{\partial\psi_2}{\partial\rho} = \frac{\partial\psi_3}{\partial\rho} \qquad \text{at } \rho = b \quad (13)$$

$$\psi_3 = \psi_0 + \psi_4; \qquad \frac{\partial\psi_3}{\partial\rho} = \frac{\partial\psi_0}{\partial\rho} + \frac{\partial\psi_4}{\partial\rho} \qquad \text{at } \rho = c. \quad (14)$$

Substituting (5), (6), (7), (9), and (11) into (12), (13), and (14) and using the orthogonality relation

$$\frac{1}{2\pi}\int_{-\infty}^{+\infty} dz\, e^{jz(k-\omega)} = \delta(k-\omega)$$

a 6×6 linear algebraic system of equations is obtained. Following tedious but straightforward algebra this system is solved and the unknown coefficients are determined. Then, assuming that the response due to the nth loop has been determined, the total response for $(2N+1)$ loops can be derived by using the superposition principle, that is,

$$\psi_i(\rho, z) = \sum_{n=-N}^{N} I_n \rho_n \int_0^{+\infty} dk\, e^{jk(z-z_n)} K_1(\mu\rho_n) F_i(k, \rho) \quad \text{for } \rho < \rho_n \quad (15)$$

where $F_i(k, \rho)$, $i = 1,2,3,4$ are given in the Appendix.

The derived field expressions are integrals of the Sommerfeld type [6]. The near-field interaction of the cylindrical object with the loop antennas prohibits the use of approximation techniques such as steepest descent or stationary phase integrations. Because of this, a numerical integration technique is employed for the computation of these integrals. A 16-point Gauss quadrature technique is used after appropriately dividing the real k axis into subsegments. Accuracy in the numerical integrations is achieved by increasing the number of segments on the real axis.

In practice it is important to estimate the radiated power from the multiloop applicator system. Then the outgoing total real power P_r from a cylindrical shell of thickness $\Delta h \to 0$ enclosing the loops is considered. Integrating the Poynting vector on the $\rho = \rho_0 - \Delta h/2$ and $\rho = \rho_0 + \Delta h/2$ surfaces, the power emitted from the loop system is found to be

$$P_r = \frac{1}{2}\mathrm{Re}\left(\int_{\varphi=0}^{2\pi} \rho_0\, d\varphi \int_{z=-\infty}^{\infty} dz \left(E_\varphi \Big|_{\rho=\rho_0+\Delta h/2} H_z^* \Big| - E \Big|_{\rho=\rho_0-\Delta h/2} H_z^* \Big| \right) \right)$$

and since

$$H_z^*\Big|_{\rho=\rho_0+\Delta h/2} - H_z^*\Big|_{\rho=\rho_0-\Delta h/2} = \int_{\rho=\rho_0-\Delta h/2}^{\rho_0+\Delta h/2} \boldsymbol{J}\cdot\hat{\varphi}\, d\rho = \sum_{n=-N}^{N} I_n^* \delta(z - z_{0n})$$

$$E_\varphi\Big|_{\rho=\rho_0+\Delta h/2} = E_\varphi\Big|_{\rho=\rho_0-\Delta h/2}$$

it is concluded that

$$P_r = \pi\rho_0 \mathrm{Re}\left\{ \sum_{n=-N}^{N} E_\varphi(\rho_0, z_{0n}) I_n^* \right\}. \quad (16)$$

III. Numerical Results and Discussion

Numerical computations have been performed by applying the theory developed in Section II. Throughout the computations the radiation frequency is taken to be 13 MHz. In Table I the dimensions and the dielectric constants [8] (see Fig. 1) employed for the cylindrical human body model are given.

In computing the integrals of (15), numerous convergence tests have been performed by increasing the Gaussian quadrature integration points. The continuity of the tangential electric field on the muscle–fat, fat–skin, and skin–air interfaces has been checked and a perfect agreement has been obtained. Since the boundary conditions on the $\rho = a$, $\rho = b$, and $\rho = c$ cylindrical surfaces are not *a priori* satisfied, this provides a good check on the correctness of the developed numerical method.

In presenting the numerical results, the normalized specific absorption rate (SAR) is considered. The SAR is computed in each case using the definition

$$SAR(\rho, z) = \frac{\sigma_i}{2\rho_m}|\boldsymbol{E}(\rho, z)|^2 \quad (17)$$

where $|E|$ is the electric field strength, $\sigma_i = \omega\epsilon_0 \mathrm{Im}(\epsilon_i)$ $(i = 1,2,3)$ is the tissue conductivity, and $\rho_m \cong 10^3$ kg/m^3 is the muscle tissue mass density. The SAR values are normalized with respect to the SAR at $\rho = c$ (21.5 cm) and $z = 0$ (i.e., the equator of the cylindrical body). The normalized SAR value $S(\rho, z)$ is defined as

$$S(\rho, z) = \frac{SAR(\rho, z)}{SAR(c, 0)}. \quad (18)$$

Furthermore, in each case the absolute value of $SAR(c,0)$ is also quoted for 500 W emitted power. To this end, (16) is used to compute the antenna currents corresponding to this commonly used power level.

In Fig. 2, results are given for a single-loop antenna of radius $\rho_0 = 32.5$ cm. The SAR (ρ, z) = constant curves are

TABLE I
HUMAN BODY PARAMETERS

Layer thickness	Dielectric constant (ϵ_i)
Muscle $a = 20$ cm	$151.852 + j948.64$
Fat $b - a = 1$ cm	$23.5 + j13.45$
Skin $c - b = 0.5$ cm	$151.852 + j948.64$

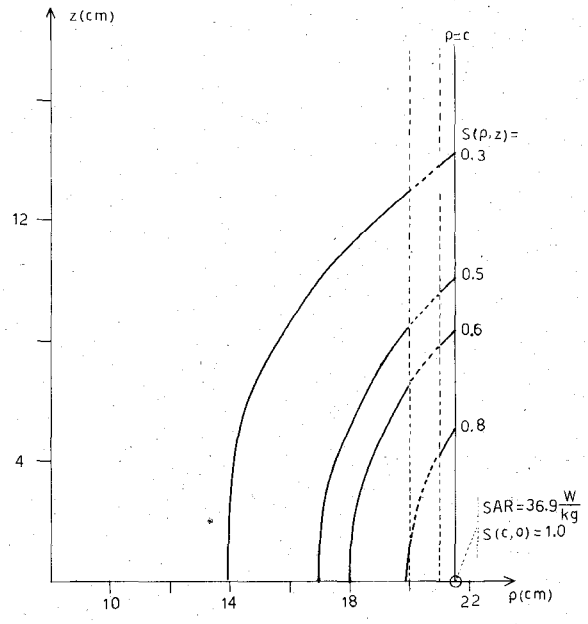

Fig. 2. Plots of iso-*SAR* curves on the (ρ, z) plane for a single-loop hyperthermia applicator of radius $\rho_0 = 32.5$ cm. The human body dimensions are defined in Table I. The loop is located on the $z = 0$ plane.

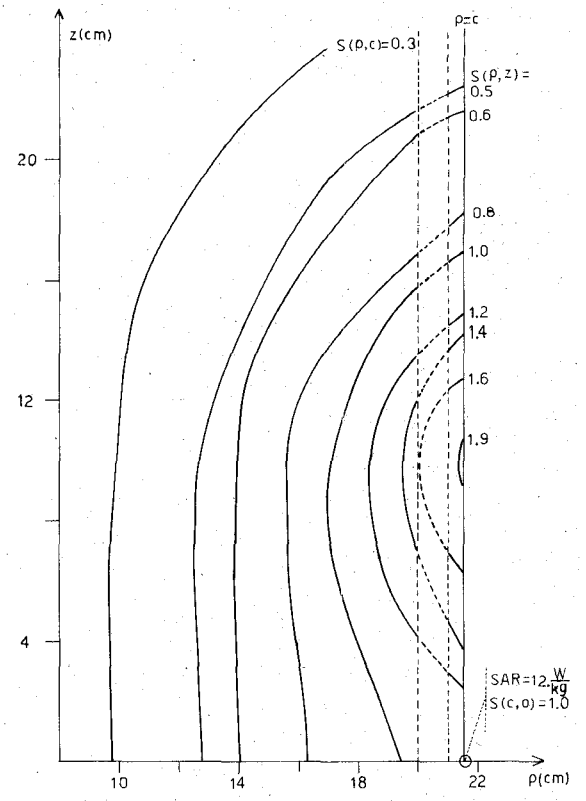

Fig. 3. *SAR* distributions for a three-element concentric loop system with $I_{-1} = I_1 = -0.577 I_0$, a common radius of loops $\rho_0 = 32.5$ cm, and a distance between successive loops along the z axis $D = 4$ cm.

plotted on the (ρ, z) plane. In order to facilitate the presentation, the low *SAR* values of the fat layer are not shown. However their values can be easily computed by multiplying the results of Fig. 2 with $\sigma_2/\sigma_1 = 0.014$ [2]. The well-known zero electric field behavior on the body axis is observed. Furthermore on the $z = 0$ loop plane, the half-power penetration depth is approximately 4.5 cm, which is in good agreement with previously published experimental results [9]. The 3 dB (half-power) zone along the body axis for a single-loop antenna is found to be approximately 20 cm. The attenuation inside the $z = 0$ plane fits approximately to the $1/\rho^2$ law, a feature which has been the main disadvantage of magnetic-loop hyperthermia applicators.

In order to achieve higher penetration depths the possibility of using several magnetic loops has been investigated. To this end three- and five-loop systems were considered. In these applicators the two outer loops (located on the $z = z_{-N}$ and $z = z_N$ planes) are fed with currents that are 180° out of phase with respect to the center loop (or loops). Through this approach it was hoped that the opposite fields due to the outer loops would suppress the strong superficial field of the center loop (or loops) and an enhancement of the power penetration depth would be achieved. Numerical results show that a significant improvement of the penetration depth can be obtained if the currents circulating on the magnetic loops have specific ratios.

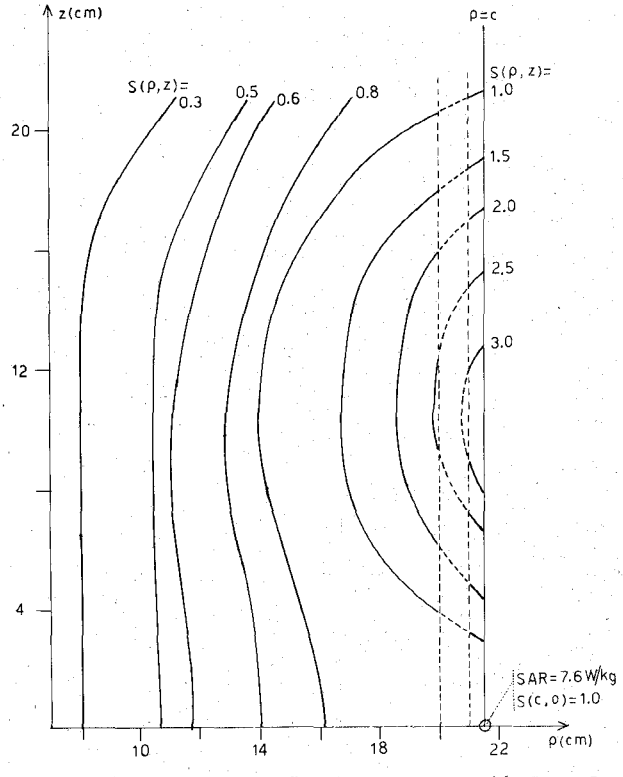

Fig. 4. *SAR* distributions for a five-element system with $I_{-2} = I_2 = -1.73 I_0$, $I_{-1} = I_1 = I_0$, $\rho_0 = 32.5$ cm, and $D = 2.5$ cm.

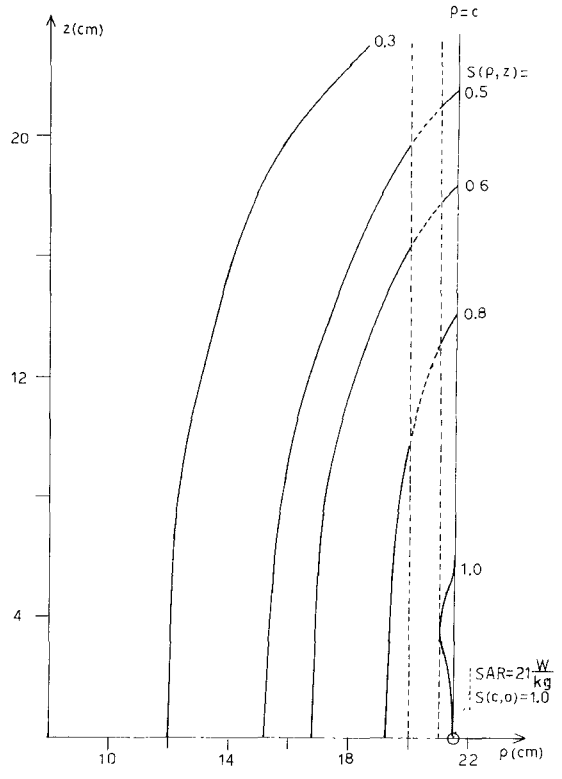

Fig. 5. *SAR* distributions for a three-loop system with $I_{-1} = I_1 = -0.59I_0$, $\rho_0 = 40$ cm, and $D = 4$ cm.

After searching *SAR* patterns with the aid of the computer, it has been found that enhanced penetration depths are obtained with the following loop arrangements.

a) three-loop system with characteristics $I_{-1} = I_1 = -0.577I_0$ and distance between successive loops along the z axis $D = 4$ cm;
b) five-loop system with $I_{-2} = I_2 = -1.73I_0$, $I_{-1} = I_1 = I_0$, and $D = 2.5$ cm.

The loop radii are all taken to be $\rho_0 = 32.5$ cm. The corresponding results are shown in Figs. 3 and 4, where the iso-*SAR* curves are given on the (ρ, z) plane. It is observed that in both cases the half-power penetration depth is considerably larger than that of the single-loop case (see Fig. 2). In the case of the five-loop system (Fig. 4), the half-power penetration depth on the $z = 0$ plane is 11 cm, while in the case of the three-loop system it is 8.7 cm. However in Fig. 4 a hot spot is observed around $z = 10$ cm limited mainly within the surface layers. Although a similar phenomenon takes place in the case of the three-element system, it is significantly less pronounced and it is restricted outside the muscle tissue. In both cases there is also an increase in the half-power zone along the body axis in comparison with the single-loop case.

Considering the absolute values of the *SAR* obtained on the $\rho = c$, $z = 0$ point, it is verified that the enhancement of the penetration depth results in a decrease of the *SAR* $(c,0)$ values for the assumed 500 W power level. This decrease in the $SAR(c,0)$ values is explained considering the fact that the power is spread into a larger muscle tissue volume.

In an effort to eliminate the hot spots observed with the proposed multiloop systems, larger radii have been considered. In Fig. 5 *SAR* patterns are shown for the case of a three-loop system with $I_{-1} = I_1 = -0.59I_0$ and $D = 4$ cm. The common loop radius is $\rho_0 = 40$ cm. In this figure no hot spots are observed but the half-power penetration depth has been reduced to 6.5 cm, while $SAR(c,0) = 21$ W/kg.

In the previous analysis the loop currents are taken to be independently adjustable. Of course in practice the strong coupling between the loops should be taken into account to achieve the desired current ratios. The 180° phase reversal can easily be obtained by using a reverse attachment to the common feeding network. The required current amplitude ratios can be obtained using either lumped reactive series elements along the outer loops or parallel coherent power amplifiers to feed each antenna.

Sensitivity analysis has been performed by varying the cylindrical human body radius to investigate whether the enhanced penetration depth holds for a wide range of human body dimensions. Numerical computations for smaller radii down to 16.5 cm show that the improved multiloop magnetic applicator is also valid.

IV. Conclusions

The power deposition into a three-layer cylindrical human body from a multiloop applicator system has been analyzed. Normalized *SAR* patterns have been computed for several loop array geometries and current excitations. A highly penetrating concentric multiloop mode of operation has been devised that is expected to provide significant improvement over the conventional single-loop applicators. The encouraging results obtained justify further research on the subject and the development of a prototype system.

Appendix

The functions $F_i(k,\rho)$, $i = 1,2,3,4$, appearing in the integrals of (15) are given by the expressions

$$F_1(k,\rho) = \frac{2}{\pi bc}\frac{1}{K_1(\mu c)} \cdot \frac{P_B(k)J_1(\lambda_2 a) - P_A(k)Y_1(\lambda_2 a)}{J_1(\lambda_1 a)} J_1(\lambda_1 \rho)$$

$$F_2(k,\rho) = \frac{2}{\pi bc}\frac{1}{K_1(\mu c)}\{P_B(k)J_1(\lambda_2\rho) - P_A(k)Y_1(\lambda_2\rho)\}$$

$$F_3(k,\rho) = \frac{1}{cK_1(\mu c)}\{(P_B(k)V_A(k) - P_A(k)W_A(k))J_1(\lambda,\rho) + (P_B(k)V_B(k) - P_A(k)W_B(k))Y_1(\lambda_3\rho)\}$$

$$F_4(k,\rho) = \frac{1}{cK_1(\mu c)}\{(P_B(k)V_A(k) - P_A(k)W_A(k))J_1(\lambda_3 c) + (P_B(k)V_B(k) - W_B(k)P_A(k))Y_1(\lambda_3 c) - j\omega\mu_0 cI_1(\mu c)K_1(\mu c)\}$$

where

$$R(k) = \mu \frac{K_1'(\mu c)}{K_1(\mu c)}$$

$$Q(k) = \lambda_1 \frac{J_1'(\lambda_1 a)}{J_1(\lambda_1 a)}$$

$$P_A(k) = \lambda_2 \cdot J_1'(\lambda_2 a) - Q(k) J_1(\lambda_2 a)$$

$$P_B(k) = \lambda_2 \cdot Y_1'(\lambda_2 a) - Q(k) Y_1(\lambda_2 a)$$

$$U_A(k) = \lambda_3 \cdot J_1'(\lambda_3 c) - R(k) J_1(\lambda_3 c)$$

$$U_B(k) = \lambda_3 \cdot Y_1'(\lambda_3 c) - R(k) Y_1(\lambda_3 c)$$

$$V_A(k) = \lambda_3 \cdot J_1(\lambda_2 b) Y_1'(\lambda_3 b) - \lambda_2 \cdot J_1'(\lambda_2 b) Y_1(\lambda_3 b)$$

$$W_A(k) = \lambda_3 \cdot Y_1(\lambda_2 b) Y_1'(\lambda_3 b) - \lambda_2 \cdot Y_1'(\lambda_2 b) Y_1(\lambda_3 b)$$

$$V_B(k) = \lambda_2 \cdot J_1'(\lambda_2 b) J_1(\lambda_3 b) - \lambda_3 \cdot J_1(\lambda_2 b) J_1'(\lambda_3 b)$$

$$W_B(k) = \lambda_2 \cdot Y_1'(\lambda_2 b) J_1(\lambda_3 b) - \lambda_3 \cdot Y_1(\lambda_2 b) J_1'(\lambda_3 b)$$

$$\Delta(k) = \left[V_A(k) \cdot U_A(k) + V_B(k) \cdot U_B(k)\right] \cdot P_B(k) - \left[W_A(k) \cdot U_A(k) + W_B(k) \cdot U_B(k)\right] \cdot P_A(k).$$

ACKNOWLEDGMENT

The authors wish to thank Mr. W. H. Harrison for his helpful suggestions.

REFERENCES

[1] J. W. Strohbehn and E. B. Douple, "Hyperthermia and cancer therapy: A review of biomedical engineering contributions and challenges," *IEEE Trans. Biomed. Eng.*, vol. BME-31, pp. 779–787, Dec. 1984.

[2] F. K. Storm, R. S. Elliott, W. H. Harrison, and D. L. Morton, "Clinical RF hyperthermia by magnetic-loop induction: A new approach to human cancer therapy," *IEEE Trans. Microwave Theory Tech.*, vol. MTT-30, pp. 1149–1158, Aug. 1982.

[3] F. K. Storm *et al.*, "Magnetic-induction hyperthermia: Results of a 5-year multi-institutional national cooperative trial in advanced cancer patients," *Cancer*, vol. 55, pp. 2677–2687, June 1, 1985.

[4] P. S. Ruggera and G. Kantor, "Development of a family of RF helical coil applicators which produce transversely uniform axially distributed heating in cylindrical fat–muscle phantoms," *IEEE Trans. Biomed. Eng.*, vol. BME-31, pp. 98–106, Jan. 1984.

[5] S. C. Hill, D. A. Christensen, and C. H. Durney, "Power deposition patterns in magnetically-induced hyperthermia: A two-dimensional quasistatic numerical analysis," *Int. J. Radiat. Biol.*, vol. 9, pp. 893–909, 1983.

[6] A. R. Sommerfeld, *Partial Differential Equations in Physics*. New York: Academic Press, 1949.

[7] P. M. Morse and F. Feshbach, *Methods in Theoretical Physics*. New York: McGraw-Hill, pt. I.

[8] A. W. Guy, C. C. Johnson, J. C. Lin, and K. K. Kraning, "Electromagnetic power deposition in man exposed to high-frequency fields and the associated thermal and physiologic consequences," Rep. SAM-TR-73-13, NTIS, U.S. Dept. of Commerce, 1973.

[9] W. H. Harrison, F. K. Storm, R. S. Elliott, and D. L. Morton, "A comparison of deep-heating electrode concepts for hyperthermia," *J. Microwave Power*, vol. 2, p. 4, 1985.

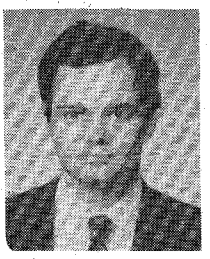

P. G. Cottis was born in Salonica, Greece, in 1956. He received the Diploma degree in electrical engineering from the National Technical University of Athens (NTUA) in 1979, the M.Sc. degree in communication engineering from the University of Manchester in 1980, and the doctor's degree in electrical engineering from NTUA in 1984.

From 1981 until 1984 he worked as a Research Associate in the Department of Electrical Engineering at NTUA. In November 1985 he joined NTUA as a Lecturer in Electrical Engineering, a position that he currently holds. His main research interest is in the electromagnetic fields area with emphasis on microwaves and fiber optics.

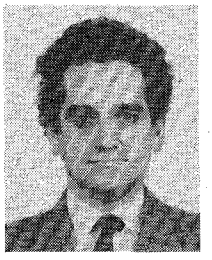

Nikolaos K. Uzunoglu (M'82) received the B.Sc. degree in electronics engineering from the Istanbul Technical University, Turkey, in 1973. He obtained the M.Sc. and Ph.D. degrees from the University of Essex, England, in 1974 and 1976, respectively.

He worked for the Hellenic Navy Research and Technology Development Office from 1977 to 1984. During this period, he also worked on a part-time basis at the National Technical University on electromagnetic theory. In 1984, he was elected Associate Professor at the National Technical University of Athens, the position that he holds presently. His research interests are microwave applications, fiber optics, and electromagnetic theory.

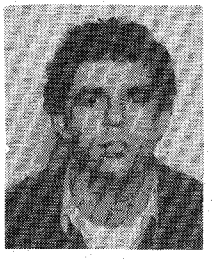

G. E. Chatzarakis was born in Serres, Greece, on May 20, 1961. He received the Diploma degree in electrical engineering from the National Technical University of Athens (NTUA) in 1986. Since 1986 he has been a postgraduate student at NTUA working in the area of microwaves.